The F-actin bundler α-actinin Ain1 is tailored for ring assembly and constriction during cytokinesis in fission yeast

Yujie Li[a], Jenna R. Christensen[b,†], Kaitlin E. Homa[b,†], Glen M. Hocky[c], Alice Fok[b], Jennifer A. Sees[b], Gregory A. Voth[c], and David R. Kovar[a,b,d,*]

[a]Committee on Genetics, Genomics and Systems Biology, [b]Department of Molecular Genetics and Cell Biology, [c]Department of Chemistry, James Franck Institute, Institute for Biophysical Dynamics, and Computation Institute, and [d]Department of Biochemistry and Molecular Biology, University of Chicago, Chicago, IL 60637

ABSTRACT **The actomyosin contractile ring is a network of cross-linked actin filaments that facilitates cytokinesis in dividing cells. Contractile ring formation has been well characterized in *Schizosaccharomyces pombe*, in which the cross-linking protein α-actinin SpAin1 bundles the actin filament network. However, the specific biochemical properties of SpAin1 and whether they are tailored for cytokinesis are not known. Therefore we purified SpAin1 and quantified its ability to dynamically bind and bundle actin filaments in vitro using a combination of bulk sedimentation assays and direct visualization by two-color total internal reflection fluorescence microscopy. We found that, while SpAin1 bundles actin filaments of mixed polarity like other α-actinins, SpAin1 has lower bundling activity and is more dynamic than human α-actinin HsACTN4. To determine whether dynamic bundling is important for cytokinesis in fission yeast, we created the less dynamic bundling mutant SpAin1(R216E). We found that dynamic bundling is critical for cytokinesis, as cells expressing SpAin1(R216E) display disorganized ring material and delays in both ring formation and constriction. Furthermore, computer simulations of initial actin filament elongation and alignment revealed that an intermediate level of cross-linking best facilitates filament alignment. Together our results demonstrate that dynamic bundling by SpAin1 is important for proper contractile ring formation and constriction.**

Monitoring Editor
Laurent Blanchoin
CEA Grenoble

Received: Jan 7, 2016
Revised: Apr 6, 2016
Accepted: Apr 6, 2016

INTRODUCTION

Filamentous actin (F-actin) is organized by a variety of actin-binding proteins to generate diverse networks that support essential cellular functions. One key structure is the bundled network, which provides cells with the stability and rigidity necessary to generate force, tension, and contraction. F-actin–bundling proteins are an important and diverse group of proteins that include fimbrin, fascin, α-actinin, formin, Ena/VASP, filamin, spectrin, villin, and espin (Otto, 1994; Bartles, 2000; Krause *et al.*, 2003; Feng and Walsh, 2004; Broderick and Winder, 2005; Breitsprecher and Goode, 2013). These F-actin bundlers create physical links between individual filaments by binding to multiple filaments simultaneously, either through multiple actin-binding domains in one monomer (such as fimbrin and fascin) or by dimerization of monomers that each contain a single actin-binding domain (such as α-actinin and spectrin; Matsudaira, 1991; Djinovic-Carugo *et al.*, 1997; Xu *et al.*, 1998; Virel and Backman, 2004; Sjoblom *et al.*, 2008).

α-Actinin is an F-actin bundler conserved across eukaryotes and belonging to the spectrin family of multidomain proteins, named after the spectrin dimerization domain (Virel and Backman, 2004; Broderick and Winder, 2005). α-Actinin functions as a dimer, with each monomer consisting of an actin-binding domain and a

This article was published online ahead of print in MBoC in Press (http://www.molbiolcell.org/cgi/doi/10.1091/mbc.E16-01-0010) on April 13, 2016.

†These authors contributed equally to this work.

*Address correspondence to: David R. Kovar (drkovar@uchicago.edu).

Abbreviations used: ABD, actin-binding domain; βME, β-mercaptoethanol; CH, calponin homology; DIC, differential interference contrast; DTT, dithiothreitol; EGTA, ethylene glycol tetraacetic acid; F-actin, filamentous actin; GFP, green fluorescent protein; HsACTN4, human α-actinin 4; SCPR, search, capture, pull, release; SR, spectrin repeat; TIRFM, total internal reflection fluorescence microscopy; TMR, tetramethyl-rhodamine; WT, wild type.

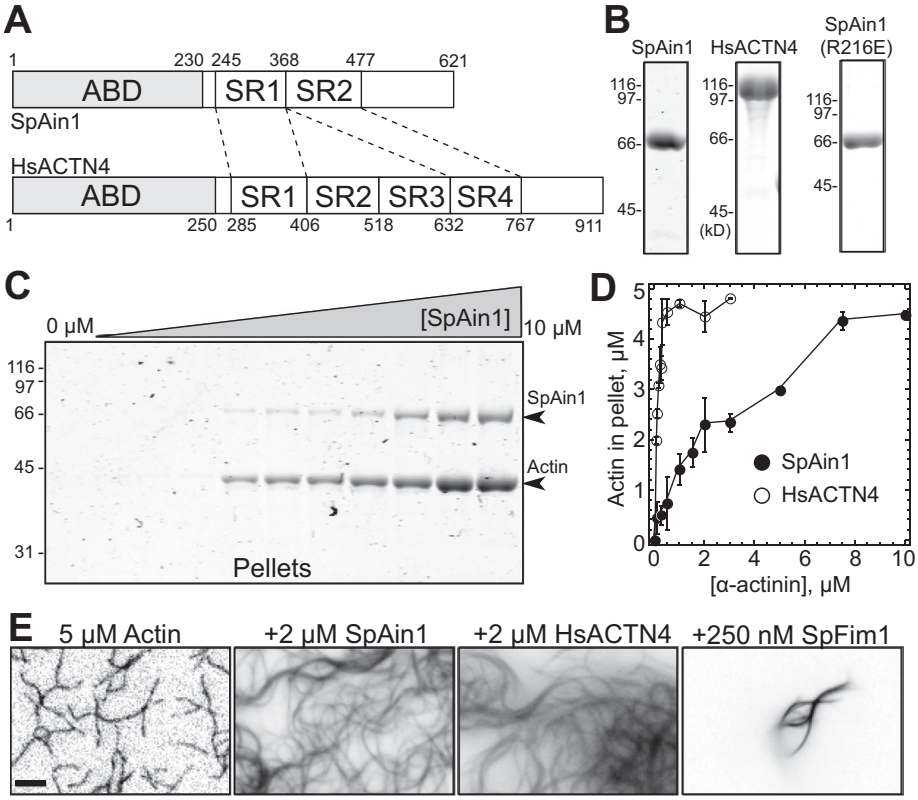

FIGURE 1: SpAin1 bundles F-actin. (A) Domain organization of fission yeast α-actinin SpAin1 and human α-actinin 4 HsACTN4, with amino acid numbers indicated next to domain boundaries. Dashed lines indicate significant residue identity between specific spectrin repeats (SR). ABD, actin-binding domain. (B) Regions of Coomassie blue–stained gels showing purified proteins used in this study. (C and D) Low-speed (10,000 × *g*) sedimentation of F-actin preassembled from 5 μM Mg-ATP actin, following incubation with a range of SpAin1 or HsACTN4 concentrations for 20 min at 25°C. (C) Coomassie blue–stained gel of pellets from a representative experiment with SpAin1. (D) Plot of the dependence of actin in the pellets on the concentration of SpAin1 or HsACTN4. Error bars, SE; $n = 3$. (E) Fluorescence micrographs of preassembled F-actin labeled with rhodamine–phalloidin following incubation with the indicated cross-linkers for 20 min. Scale bar: 5 μm.

dimerization domain of one to four spectrin repeats (SRs; Matsudaira, 1991; Djinovic-Carugo *et al.*, 1997, 1999; Virel and Backman, 2004, 2007). α-Actinin has been implicated in a broad range of cellular processes such as muscle formation (Broderick and Winder, 2005), motility (Honda *et al.*, 2005; Shao *et al.*, 2010), and adhesion (Rajfur *et al.*, 2002; Dandapani *et al.*, 2007; Tang and Brieher, 2012; Roca-Cusachs *et al.*, 2013), and both skeletal and nonskeletal muscle α-actinin bind and bundle F-actin (Wachsstock *et al.*, 1993; Virel and Backman, 2006; Weins *et al.*, 2007; Courson and Rock, 2010; Low *et al.*, 2010; Foley and Young, 2013). Additionally, α-actinins have been found in the division plane or cleavage furrow in both mammalian cell tissues and sea urchin embryos and are required for F-actin remodeling throughout cytokinesis in epithelial cells (Fujiwara *et al.*, 1978; Mabuchi *et al.*, 1985; Sanger *et al.*, 1987; Mukhina *et al.*, 2007).

Animal cells often express multiple α-actinin isoforms that are involved in diverse roles. Conversely, the fission yeast *Schizosaccharomyces pombe* expresses one α-actinin isoform, Ain1 (hereafter SpAin1), which is primarily involved in cell division (Wu *et al.*, 2001). Fission yeast offers many advantages for studying α-actinin in cytokinesis, including convenient genetic manipulation, a relatively small number of conserved ring components, and high temporal resolution of cytokinetic events. Extensive studies of *S. pombe* cytokinesis have resulted in the search, capture, pull, release (SCPR) model for node coalescence, which proposes that formin Cdc12 located in pre ring nodes generates F-actin that is captured and pulled by myosin II in adjacent nodes, allowing for filament bundling and condensation of the network to form a compact ring (Wu *et al.*, 2003, 2006; Vavylonis *et al.*, 2008; Coffman *et al.*, 2009; Ojkic and Vavylonis, 2010; Ojkic *et al.*, 2011).

The role of SpAin1 in cytokinesis has been investigated using a combination of genetics, live-cell imaging, and mathematical modeling (Wu *et al.*, 2001; Laporte *et al.*, 2012; Bidone *et al.*, 2014; Stachowiak *et al.*, 2014). However, these studies have assumed that SpAin1 is a dynamic cross-linking protein that bundles F-actin with mixed orientations based on its similarity to other α-actinins and localization to the division site. Although SpAin1 was recently shown to bind and bundle F-actin (Addario *et al.*, 2016), the quantitative behavior of SpAin1 on single and bundled actin filaments, the properties of SpAin1-mediated bundles, and whether these properties are critical for SpAin1's roles in cytokinesis remain unknown. We therefore purified SpAin1, extensively quantified the dynamic F-actin–binding and –bundling properties of SpAin1, and created an enhanced bundling mutant, which allowed us to directly investigate the in vivo consequences of modulating SpAin1's bundling activity. Our results not only provide several lines of evidence supporting previous studies and simulations but also demonstrate that perturbation of SpAin1's intrinsic bundling properties results in severe cytokinetic defects, indicating the importance of maintaining an optimized level of balanced bundling activity for cell division.

RESULTS

Fission yeast α-actinin SpAin1 binds and bundles F-actin

The fission yeast α-actinin protein SpAin1 was initially identified based on sequence homology. While it was previously shown to localize to the contractile ring and cause cytokinetic defects when deleted (Wu *et al.*, 2001), recent genetic, cell biological, and mathematical studies have proposed that a balanced amount of SpAin1 bundling activity is important for both assembly and constriction of the contractile ring (Laporte *et al.*, 2012; Mishra *et al.*, 2013; Stachowiak *et al.*, 2014). Therefore we sought to purify SpAin1 and directly compare its quantitative F-actin–binding and F-actin–bundling properties with those of the well-characterized human α-actinin 4 (hereafter HsACTN4; Kaplan *et al.*, 2000; Weins *et al.*, 2005, 2007).

SpAin1 and HsACTN4 have similar overall domain organizations (Figure 1A). Each contains an N-terminal F-actin–binding domain composed of two calponin homology (CH) domains. Each also contains SRs that facilitate formation of antiparallel homodimers (Figure 1A and Supplemental Figure S1A; Blanchard *et al.*, 1989; Djinovic-Carugo *et al.*, 1999; Ylanne *et al.*, 2001). While HsACTN4 contains

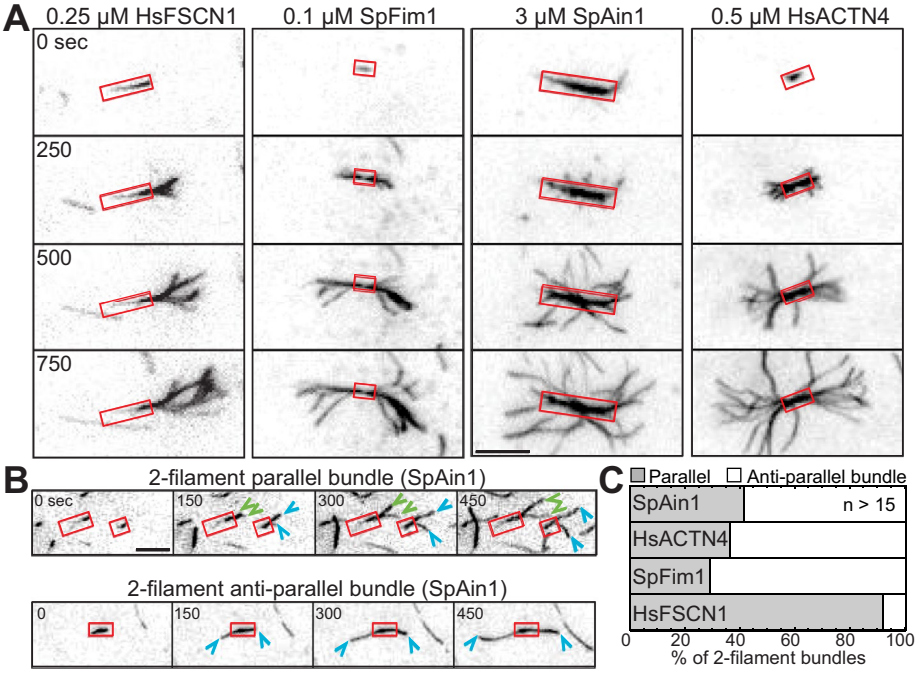

FIGURE 2: SpAin1 makes F-actin bundles of mixed polarity. (A–C) TIRFM observation of the addition of 0.75 μM Mg-ATP actin (33.3% Oregon Green-actin) to preassembled F-actin bundles (red boxes) (10.0% Oregon Green-actin) made by the indicated concentrations of human fascin HsFSCN1, fission yeast fimbrin SpFim1, SpAin1, or HsACTN4. (A) Time-lapse fluorescence micrographs. Scale bar: 5 μm. (B) Time-lapse fluorescence micrographs of representative parallel (top) and antiparallel (bottom) two-filament bundles made by SpAin1, used for quantification in C. Scale bar: 5 μm. Green and blue arrowheads mark F-actin barbed ends. (C) Percentage of two-filament bundles that are parallel and antiparallel.

four SRs, SpAin1 has only two, which are most similar to SR1 and SR4 of HsACTN4 (Supplemental Figure S1, C and D). Though HsACTN4 can be purified from *Escherichia coli*, SpAin1 is poorly expressed in both *E. coli* and *S. pombe* and was therefore purified from an insect cell expression system (Figure 1B; *Materials and Methods*).

We first used cosedimentation assays to compare the relative abilities of SpAin1 and HsACTN4 to bind and bundle F-actin. SpAin1 binds and sediments with F-actin following high-speed ultracentrifugation at 100,000 × *g* (Supplemental Figure S2A). Curve fits of the amount of SpAin1 bound over a range of actin concentrations suggest an apparent affinity ($K_{d\ app}$) of 4.3 μM, although we were unable to saturate the binding reaction (Supplemental Figure S2B). Furthermore, a range of concentrations of either SpAin1 or HsACTN4 increases the amount of F-actin that pellets in low-speed sedimentation assays at 10,000 × *g*, indicating that SpAin1 is capable of cross-linking F-actin (Figure 1, C and D). However, HsACTN4 is a better bundler than SpAin1, as at least eightfold more SpAin1 is required to sediment 5 μM preassembled F-actin to the same extent (Figure 1D). Similar to previously characterized fission yeast fimbrin SpFim1 (Nakano *et al.*, 2001; Wu *et al.*, 2001; Skau *et al.*, 2009; Skau and Kovar, 2010), SpAin1 forms bundles by visualizing F-actin labeled with rhodamine–phalloidin in the absence and presence of SpAin1 and HsACTN4 (Figure 1E).

SpAin1 bundles filaments of mixed polarity

Most α-actinins form F-actin bundles composed of filaments with mixed polarities (Meyer and Aebi, 1990; Taylor *et al.*, 2000; Liu *et al.*, 2004; Hampton *et al.*, 2007; Courson and Rock, 2010). Actin filaments in the fission yeast contractile ring are of mixed polarity (Kamasaki *et al.*, 2007), and the SCPR model for contractile ring assembly in fission yeast suggests that SpAin1 must make both parallel and antiparallel F-actin bundles to align diffusing filaments (Ojkic *et al.*, 2011; Laporte *et al.*, 2012; Stachowiak *et al.*, 2014). We determined the polarity of F-actin in bundles assembled by SpAin1 by using total internal reflection fluorescence microscopy (TIRFM) to directly visualize the elongation of filaments from preassembled bundles (Figure 2 and Supplemental Videos 1 and 2). F-actin (10% Oregon Green-actin) was preassembled in the presence of bundling proteins. New "brighter" Mg-ATP actin monomer (33% Oregon Green-actin) was then flowed into the reaction chamber, and the direction of elongation was used to determine the polarity of the bundled filaments.

Human fascin HsFSCN1, which makes bundles with exclusively parallel filaments (Ishikawa *et al.*, 2003; Courson and Rock, 2010), generates seeds from which filaments elongate solely from one end (Figure 2A and Supplemental Video 1). Conversely, the versatile cross-linker SpFim1 generates seeds that elongate from both ends (Figure 2A; Skau *et al.*, 2011). Similarly, both HsACTN4 and SpAin1 assemble bundles composed of filaments with mixed orientations, as filaments elongate from both ends of preassembled seeds (Figure 2A). We quantified the polarity of filaments in preassembled two-filament bundles (Figure 2B and Supplemental Video 2). Greater than 90% of filaments elongated from fascin bundles are parallel, while SpFim1, SpAin1, and HsACTN4 make bundles with either parallel or antiparallel filaments (Figure 2C). The polarity of bundles is unaffected by bundler concentration, since HsACTN4 assembles bundles of similar mixed polarity from a range of concentrations from 10 to 100 nM (unpublished data).

SpAin1 forms fewer bundled filaments than HsACTN4

We used two-color TIRFM to monitor the formation and dynamics of bundles and to visualize and characterize the decoration of SpAin1 on individual and bundled filaments. We labeled WT SpAin1 and determined by low-speed sedimentation and TIRFM analysis that it bundles filaments to the same degree as unlabeled SpAin1 (Supplementary Figure S3). We then assembled Mg-ATP actin (33% Oregon Green-actin) in the presence of SpAin1 (20% tetramethyl-rhodamine [TMR]-labeled). In a typical bundling event, one filament collides with another by diffusion, and they subsequently align and elongate together (Figure 3A and Supplemental Video 3). Interestingly, SpAin1 does not decorate individual filaments well but significantly accumulates along F-actin bundles.

TIRFM allowed us to quantify the amount of bundles formed over time (Figure 3, B–D and Supplemental Video 4). In control reactions without α-actinin, Mg-ATP actin (33.3% Oregon Green-actin) spontaneously assembles into individual filaments (Figure 3B, left panels). Occasionally, these control filaments cross over, but they are quickly separated by diffusion, since they are not physically linked. In the presence of 100 nM HsACTN4 (Figure 3B, middle panels) or 100 nM SpAin1 (Figure 3B, right panels), some filaments

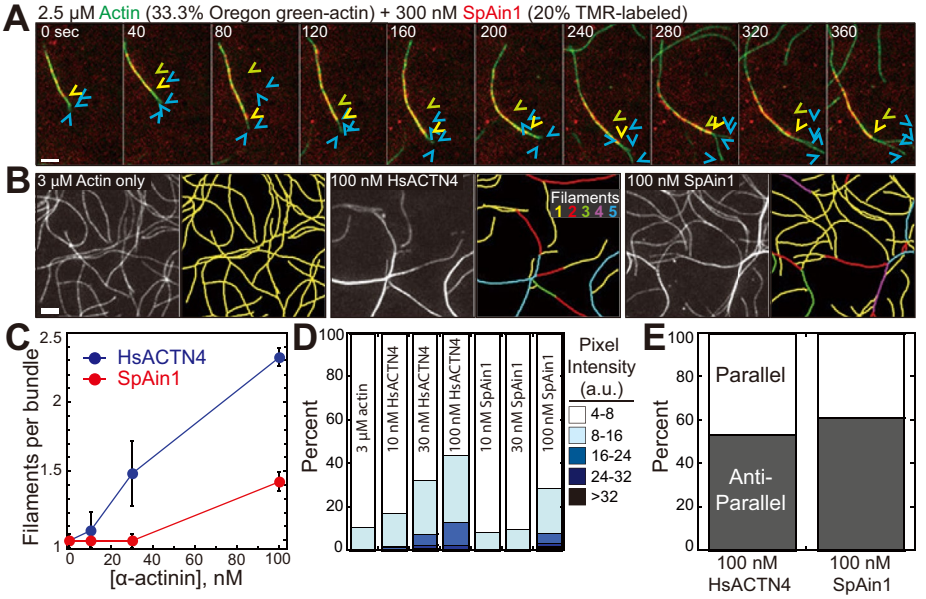

FIGURE 3: SpAin1 bundles F-actin less well than HsACTN4. (A) Merged two-color TIRFM time-lapse fluorescence micrographs showing the assembly of 2.5 μM Mg-ATP actin (33.3% Oregon Green-actin) in the presence of 300 nM SpAin1 (20% labeled with TMR). Blue and yellow arrowheads mark elongating barbed ends and SpAin1 decoration of a two-filament bundle. Scale bar: 5 μm. (B–E) Single-color TIRFM of the assembly of 2.5 μM Mg-ATP actin (33.3% Oregon Green-actin) in the absence and presence of the indicated concentrations of HsACTN4 or SpAin1. (B) Representative field of filaments 12 min after reactions were initiated. Fluorescence micrographs (left) and pseudocolored panels (right) with individual and bundled filaments traced with different colors: yellow, 1 filament; red, 2; green, 3; magenta, 4; cyan, ≥ 5. Scale bar: 5 μm. (C) Dependence of the number of filaments per bundle on the concentration of SpAin1 or HsACTN4. Error bars, SE; $n = 4$. (D) Distribution of Oregon Green-actin pixel intensity of filaments assembled in the absence and presence of SpAin1 or HsACTN4. (E) Polarity of two-filament bundles.

become permanently aligned into higher-order bundles when they encounter each other, and the barbed end of one filament then elongates along the side of the other filament. We compared the bundling abilities of SpAin1 and HsACTN4 by measuring the filament density of bundles 12 min after the assembly reactions were initiated. Filament densities were determined two ways. First, we tracked the history of bundle formation manually over time, which allowed us to distinguish up to bundles of five filaments (Figure 3, B, pseudocolored images, and C). Second, we measured the Oregon Green fluorescence intensity per pixel along the filament length, which assumes a linear correlation between pixel intensity and filament number (Figure 3D). By both measurement methods, HsACTN4 and SpAin1 bundle F-actin. However, HsACTN4 makes significantly more bundles than SpAin1 over a range of concentrations. Furthermore, in agreement with seeded TIRFM experiments (Figure 2), by tracking the direction of elongation of filaments in bundles, we determined that both SpAin1 and HsACTN4 make bundles composed of filaments of mixed polarities (Figure 3E).

SpAin1 associates with F-actin more dynamically than HsACTN4

We next sought to understand what accounts for the lower bundling activity of SpAin1 compared with HsACTN4. One major difference between these α-actinins is the number of SRs that facilitate their dimerization (Figure 1A). SpAin1 contains two SRs, whereas HsACTN4 contains four SRs, raising the possibility that SpAin1 might be a less active bundler because it dimerizes poorly. However, both SpAin1 and HsACTN4 elute in single peaks from a gel filtration column, corresponding to the predicted size of their respective dimers (Supplemental Figure S4).

Another possibility is that SpAin1's lower bundling activity is due to intrinsic properties of its actin-binding domain (ABD). We therefore performed rapid acquisition (frame rate = 0.1 s) TIRFM imaging with Oregon Green–labeled actin and TMR-labeled SpAin1 or HsACTN4. Only 1% of the α-actinin was labeled, allowing observation of individual fluorescent speckles. F-actin was spontaneously assembled from Mg-ATP actin (33.3% Oregon Green-actin) until two-filament (Figure 4 and Supplemental Video 5) and three-filament (Supplemental Figure S5 and Supplemental Video 6) bundles formed that were decorated with α-actinin speckles. Merged fluorescence micrographs (Figure 4A and Supplemental Figure S5A) and associated time-lapse fluorescence micrographs (Figure 4B and Supplemental Figure S5B) and kymographs (Figure 4C and Supplemental Figure S5C) revealed the characteristics of individual α-actinin speckles. HsACTN4 speckles remain on two- and three-filament bundles for multiple seconds with relatively few new binding and unbinding events. By comparison, new SpAin1 speckles appear often and have a significantly shorter lifetime on both two- and three-filament bundles. Histograms of α-actinin speckle residence times (Figure 4D) and associated exponential fits of the fraction of α-actinin bound over time (Figure 4E) revealed that SpAin1 is ~25-fold more dynamic (higher on and off rate) than HsACTN4. HsACTN4 speckles have an average residence time of 6.2 and 10.6 s on two- and three-filament bundles. By comparison, SpAin1 speckles have an average residence time of ~0.3 s on both two- and three-filament bundles. Because both α-actinins are potentially TMR-labeled at multiple cysteine residues, six in SpAin1 and eight in HsACTN4, direct measurement of molecule number by fluorescence intensity is difficult. However, there is little correlation between fluorescence intensity and residence duration for both SpAin1 and HsACTN4 on either two- or three-filament bundles (Supplemental Figure S6).

A SpAin1 point mutation that increases its residence time and bundling activity

We hypothesized that SpAin1's short residence time on F-actin bundles directly results in the observed lower bundling activity. We tested this possibility by characterizing the properties of a specific point mutant SpAin1(R216E) (Figure 5A and Supplemental Figure S1B). The corresponding mutation in a human α-actinin, HsACTN4(K255E), has a higher affinity for F-actin and increased bundling activity compared with wild-type (WT) HsACTN4 (Weins *et al.*, 2007; Ward *et al.*, 2008). The mutated basic lysine is a highly conserved residue located in the last α-helix of CH2 of the ABD (Figure 5A and Supplemental Figure S1B; Borrego-Diaz *et al.*, 2006). Structural studies revealed that this residue is within a region that governs activation of the ABD by releasing an inhibitory effect of CH2 on CH1 (Galkin *et al.*, 2010).

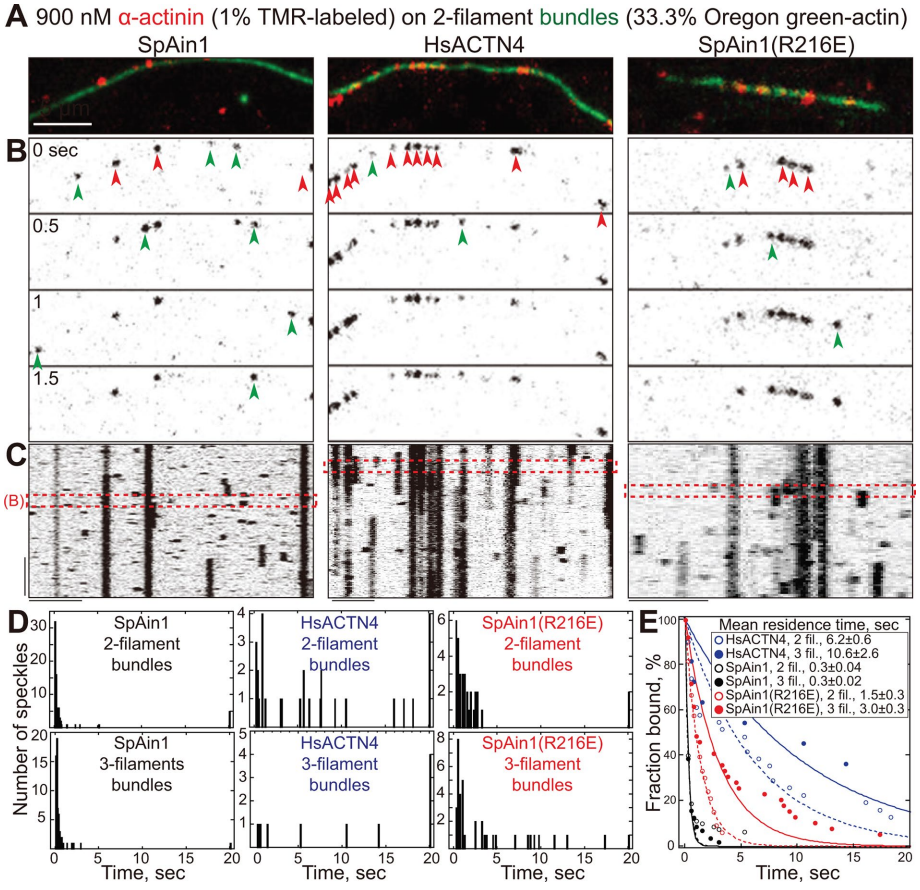

FIGURE 4: SpAin1 is a highly dynamic F-actin–bundling protein. (A–E) Two-color TIRFM of 2.5 µM Mg-ATP actin (33.3% Oregon Green-actin) assembled in the presence of 900 nM SpAin1, HsACTN4 or SpAin1(R216E) (1% TMR-labeled). (A) Merged fluorescence micrographs of α-actinin on two-filament bundles. Scale bar: 5 µm. (B) Time-lapse fluorescence micrographs of TMR-labeled α-actinin on corresponding bundles in A. Arrowheads mark speckles that remain for more (red) or less (green) than 1.5 s. (C) Kymographs of α-actinin on bundles in A over 20 s. Red boxes mark the 1.5 s of montages shown in B. Scale bars: 5 µm (horizontal); 5 s (vertical). (D) Histograms of the residence time of α-actinin speckles on two- and three-filament bundles. (E) Exponential fits of the fraction of α-actinin bound over time on two- and three-filament bundles, revealing the indicated residence times.

In rapid-acquisition TIRFM assays, the residence time of individual TMR-labeled SpAin1(R216E) speckles on Oregon Green–labeled two- and three-filament bundles (Figure 4, A–C, right panels, and Supplemental Figure S5, A–C, right panels) is 5- and 10-fold longer than that of WT SpAin1 (Figure 4, D and E). Consequently, SpAin1(R216E) is a significantly more active bundling protein than WT SpAin1. Similar to WT SpAin1, SpAin1(R216E) produces bundles with filaments of mixed polarity (Figure 5E). However, approximately fourfold less SpAin1(R216E) is required to sediment the same amount of F-actin at low speed (Figure 5B), and SpAin1(R216E) increases the average number of filaments per bundle visualized by TIRFM (Figure 5, C and D, and Supplemental Video 7). These findings suggest that increased residence time on actin bundles results in increased F-actin bundling.

Overexpression of the SpAin1(R216E) mutant causes severe cytokinetic defects

To determine whether the specific F-actin–bundling properties of SpAin1 are critical for cytokinesis in fission yeast, we characterized cells in which the endogenous SpAin1 was deleted and either SpAin1–green fluorescent protein (SpAin1-GFP) or the mutant SpAin1(R216E)-GFP was expressed at varying levels. SpAin1 null cells (*ain1-Δ1*) expressing either WT SpAin1-GFP or mutant SpAin1(R216E)-GFP under control of either the low- (*81nmt1*) or medium- (*41nmt1*) strength thiamine-repressible promoter were generated (Figure 6). Expression levels were quantified by the global GFP fluorescence determined from compiled z-stack images (Figure 6D). SpAin1-GFP and SpAin1(R216E)-GFP expressed from the low-strength (*81nmt*) promoter were each expressed approximately twofold less than SpAin1-GFP expressed from the endogenous promoter, whereas SpAin1-GFP and SpAin1(R216E)-GFP expressed from the medium-strength (*41nmt*) promoter were both expressed approximately fivefold more than endogenous (similar to previous reports by Laporte *et al.* [2012]).

The general morphology of fission yeast cells and their ability to divide properly was determined by staining with 4,6-diamidino-2-phenylindole (DAPI) and calcofluor to visualize nuclei and septa (Figure 6A). Twenty-four hours after removal of thiamine, all strains expressing SpAin1-GFP show a phenotype similar to WT, with ~20–30% binucleate cells and nearly 100% normal septa (Figure 6, A and B). Though cells expressing the mutant SpAin1(R216E)-GFP at low strength also have normal nuclei and septa, cells expressing SpAin1(R216E)-GFP from the medium-strength promoter display severe cytokinetic defects, with ~80% of cells containing two or more nuclei, and ~80% containing misaligned, excessive, and/or aggregated septa. Under all expression levels, both SpAin1-GFP and SpAin1(R216E)-GFP colocalize with contractile ring material labeled by the myosin-II regulatory light chain Rlc1-tdTomato (Figure 6C). However, while cells expressing SpAin1-GFP from the medium-strength promoter show normal rings decorated with SpAin1, all cells expressing SpAin1(R216E)-GFP at a similar level have dense and disorganized ring structures spread over a broad region near the middle of the cell (Figure 6C). These results indicate that dynamic F-actin bundling by WT SpAin1 is critical for successful cytokinesis.

Mutant SpAin1(R216E) delays both ring assembly and ring constriction

We determined the stages of cytokinesis that require dynamic F-actin bundling by imaging live cells over time using differential interference contrast (DIC) and fluorescence microscopy of Rlc1-tdTomato–labeled contractile rings (Figure 7, Supplemental Figure S7, and Supplemental Video 8). The time course of the primary pathway for contractile ring assembly and constriction in fission yeast is remarkably stereotyped in a coordinated progression of major events (Wu *et al.*, 2003, 2006): 1) Initial appearance of cytokinetic node material (start), 2) completion of ring assembly, 3) constriction initiation, 4) constriction completion, 5) disappearance of contractile ring components, and 6) cell separation (abscission) (Supplemental Figure S7C).

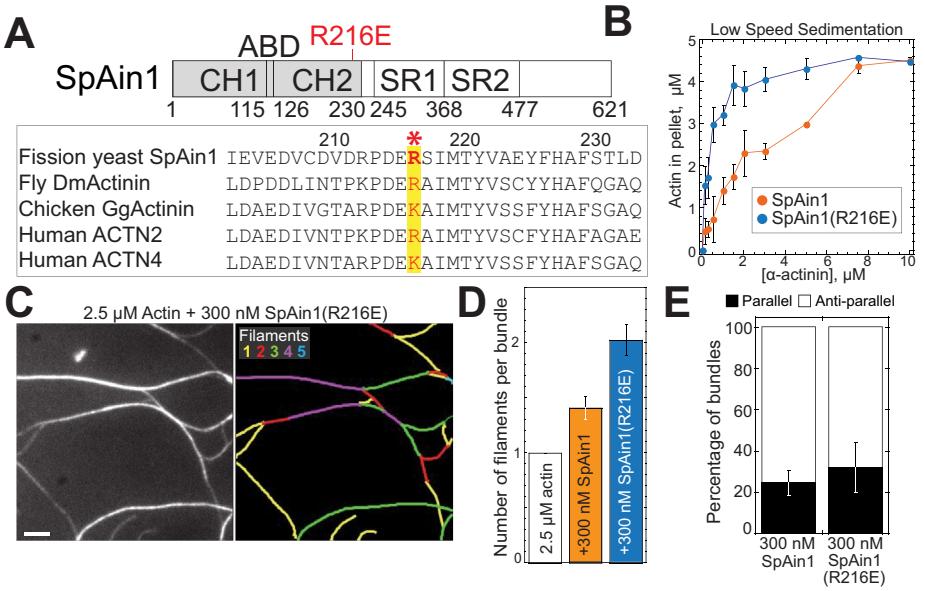

FIGURE 5: Mutant SpAin1(R216E) bundles F-actin better than WT SpAin1. (A) Domain organization of SpAin1 indicating the position of the R216E mutation in the second of two CH domains (top). ABD, actin-binding domain; CH, calponin homology domain. Alignment of the last α-helix of the CH2 domain of α-actinin from different species, with the 100% conserved residue SpAin1 R216 labeled in red with an asterisk (bottom) (Borrego-Diaz *et al.*, 2006; Weins *et al.*, 2007). (B) Low-speed sedimentation of F-actin over a range of concentrations of SpAin1 or SpAin1(R216E). Error bars, SE; $n = 3$. (C and D) Single-color TIRFM of the assembly of 2.5 μM Mg-ATP actin (33.3% Oregon Green-actin) in the absence and presence of 300 nM SpAin1 or SpAin1(R216E). (C) Representative field of filaments 10 min after a reaction with SpAin1(R216E). Fluorescence micrograph (left) and pseudocolored panel (right) with individual and bundled filaments traced with different colors: yellow, 1 filament; red, 2; green, 3; magenta, 4; cyan, ≥ 5. Scale bar: 5 μm. (D) Average number of filaments per bundle. Error bars, SE; $n = 4$. (E) Quantification of bundle polarity of 300 nM WT SpAin1 or mutant SpAin1 (R216E). Error bars, SE; $n = 2$.

We measured the kinetics of cytokinesis in wild-type cells, *ain1-Δ1* cells, *ain1-Δ1* cells expressing SpAin1-GFP or SpAin1(R216E)-GFP from the medium-strength (*41nmt1*) promoter for 24 h, and *ain1-Δ1* cells expressing SpAin1-GFP or SpAin1(R216E)-GFP from the low-strength (*81nmt1*) promoter for 24 h (Figure 7, A–D, and Supplemental Figure S7, A and B).

Major differences in cytokinesis occur primarily during contractile ring assembly and constriction (Supplemental Figure S7C). Wild-type cells take ~17 min to assemble a contractile ring, while ring assembly takes ~35 min in cells expressing SpAin1(R216E) at either expression level (Figure 7E). Node organization is also disrupted, as cytokinetic nodes are evenly distributed throughout the medial cortex during ring assembly in wild-type cells (Figure 7A), while nodes in cells expressing SpAin1(R216E)-GFP from both the low- and medium-strength promoters are broadly and unevenly distributed (Figure 7D and Supplemental Figure S7B, blue arrowheads). Furthermore, cells expressing SpAin1(R216E) from the medium-strength *41nmt1* promoter appear to have more severe contractile ring assembly defects and often form linear, stable, and excessive contractile ring material (Figure 7D, green arrowheads).

Contractile ring constriction takes ~18 min in wild-type cells, and constriction is only slightly slowed in *ain1-Δ1* cells (~25 min) or *ain1-Δ1* cells expressing WT SpAin1-GFP from either promoter (~23-25 min) (Figure 7F). Furthermore, constriction is not significantly slowed in cells expressing mutant SpAin1(R216E) from the weaker (*81nmt1*) promoter (~27 min; Figure 7F). However, ring constriction is severely compromised in cells expressing SpAin1(R216E)-GFP from the medium-strength promoter (~80 min) (Figure 7F), and daughter cell separation fails in >80% of these cells (Supplemental Figure S7C). Together these results reveal that normal contractile ring formation and constriction both require dynamic SpAin1-mediated F-actin bundles (Laporte *et al.*, 2012; Mishra *et al.*, 2013; Stachowiak *et al.*, 2014).

DISCUSSION

Fission yeast is an important model for cytokinesis in eukaryotes, as contractile ring assembly and constriction have been investigated with complementary approaches: 1) genetic manipulation and identification of participating components, 2) quantitative live-cell time-lapse fluorescence microscopy, 3) in vitro characterization of purified components, and 4) the application of mathematical models (Bathe and Chang, 2009; Goyal *et al.*, 2011; Lee *et al.*, 2012). SpAin1 localizes to the contractile ring, and both deletion and high-level overexpression of SpAin1 can cause contractile ring assembly and constriction defects (Nakano *et al.*, 2001; Wu *et al.*, 2001; Laporte *et al.*, 2012; Mishra *et al.*, 2013). However, the quantitative biochemical properties of SpAin1 had not been elucidated as extensively as other key fission yeast cytokinetic proteins such as formin Cdc12 (Kovar *et al.*, 2003), myosin-II Myo2 (Lord and Pollard, 2004), anillin-like Mid1 (Saha and Pollard, 2012; Sun *et al.*, 2015), fimbrin Fim1 (Nakano *et al.*, 2001; Skau *et al.*, 2011), profilin Cdc3 (Lu and Pollard, 2001), and cofilin Adf1 (Andrianantoandro and Pollard, 2006). However, detailed mathematical models for contractile ring assembly and constriction have been built that feature dynamic bundling proteins (Laporte *et al.*, 2012; Bidone *et al.*, 2014; Stachowiak *et al.*, 2014), properties that, until now, had been only assumed or estimated based on fluorescence recovery after photobleaching studies of fluorescently labeled SpAin1 in live cells (Laporte *et al.*, 2012). We purified and characterized fission yeast α-actinin SpAin1 and determined that it is an F-actin–binding protein that dynamically bundles filaments of mixed polarity. Furthermore, through in vitro and in vivo characterization of a less dynamic SpAin1(R216E) mutant with increased bundling activity, we demonstrated that the ability of SpAin1 to dynamically bind and bundle F-actin is important for both contractile ring assembly and constriction during cytokinesis in fission yeast.

Why is a dynamic cross-linker optimal for contractile ring assembly?

Dynamic F-actin bundling by α-actinin is critical for cytokinesis in fission yeast. This study in combination with others has shown that an excess of bundling causes severe defects in contractile ring assembly and constriction, regardless of whether this excessive bundling is achieved by highly overexpressing the dynamic WT SpAin1 (Wu *et al.*, 2001; Laporte *et al.*, 2012), by expressing the less dynamic and more active bundling mutant SpAin1(R216E) (this study), or by adding exogenous bundling proteins to purified contractile rings (Mishra *et al.*, 2013).

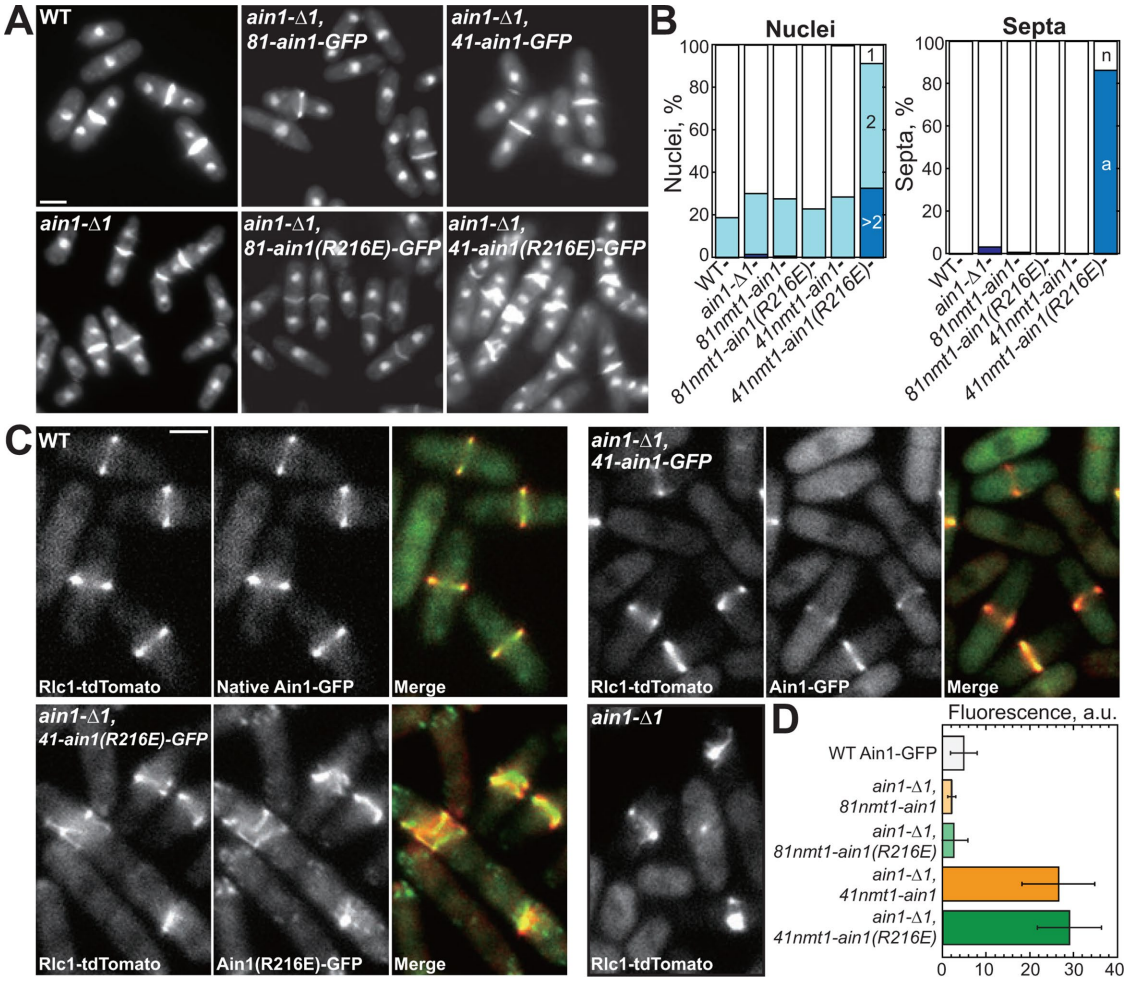

FIGURE 6: SpAin1(R216) causes severe cytokinetic defects in fission yeast. (A–D) WT cells, SpAin1 null *ain1-Δ1* cells, and *ain1-Δ1* cells expressing either WT SpAin1-GFP or mutant SpAin1(R216E)-GFP from low- (*81nmt1*) and medium- (*41nmt1*) strength promoters integrated at the *leu* locus. (A and B) General cytokinetic defects 24 h after *nmt1*-promoter induction by removal of thiamine. (A) Fluorescence micrographs of cells stained with DAPI and calcofluor to visualize nuclei and septa. (B, left) Percentage of cells with 1 (white), 2 (light blue), or > 2 nuclei (dark blue). $n \geq 400$ cells. (B, right) Percentage of normal (n, white) and abnormal (a, blue) septa. $n \geq 100$ septa. (C) Z-projection fluorescence micrographs of the indicated cells expressing the contractile ring marker Rlc1-tdTomato (left), SpAin1-GFP or SpAin1(R216E)-GFP (middle), and merge (right). Scale bar: 5 μm. (D) SpAin1-GFP and SpAin1(R216E)-GFP whole cell fluorescence for the indicated strains. Error bars, SE; $n \geq 10$ cells.

We propose that dynamic SpAin1-mediated bundling helps organize the F-actin network during ring assembly (Figure 8A; Laporte *et al.*, 2012). According to the SCPR model (Vavylonis *et al.*, 2008), the contractile ring is assembled through stochastic cycles of pre–ring node condensation. Nodes are initiated as a broad band at the cortex of the division site. Each node contains the formin Cdc12, which processively assembles F-actin, and the myosin motor Myo2, which captures actin filaments on nearby nodes and subsequently pulls nodes together (Wu *et al.*, 2003, 2006; Vavylonis *et al.*, 2008; Coffman *et al.*, 2009; Ojkic and Vavylonis, 2010; Ojkic *et al.*, 2011). Cofilin breaks transient node connections by severing filaments (Chen and Pollard, 2011), and the cycle repeats until a uniform contractile ring is formed.

We found that dynamic SpAin1 bundling is important specifically at the stage of node condensation. Our model of the importance of a dynamic cross-linker is as follows: at the beginning stages of ring assembly, actin filaments are nucleated at random orientations from nodes (Figure 8Ai), and SpAin1 bundling helps align filaments from different nodes. Although SpAin1 can generate both parallel and antiparallel bundles, antiparallel bundles are especially important, as this arrangement can help guide filament growth toward neighboring nodes for capture by myosin II (Figure 8Aii). In the absence of SpAin1, randomly generated filaments may take longer to align, compromising filament capture by myosin II and resulting in clumped ring material observed both in vivo and via three-dimensional contractile ring models (Laporte *et al.*, 2012; Bidone *et al.*, 2014). On the other hand, excessive bundling by the less dynamic SpAin1(R216E) may prevent filaments from reaching neighboring nodes (Figure 8B, i–iii), resulting in an unproductive "meshwork" instead of a condensed contractile ring (Figure 8Biii). An intermediate level of bundling promoted by the dynamic nature of SpAin1 allows for increased filament alignment and improved connections between neighboring myosin-II nodes without the adverse effects caused by excessive bundling.

To test whether a dynamic cross-linker decreases the time to actin filament capture by myosin II, we adapted a model to simulate actin filament elongation and capture by two neighboring nodes (Laporte *et al.*, 2012). We varied the dynamicity of cross-linkers by

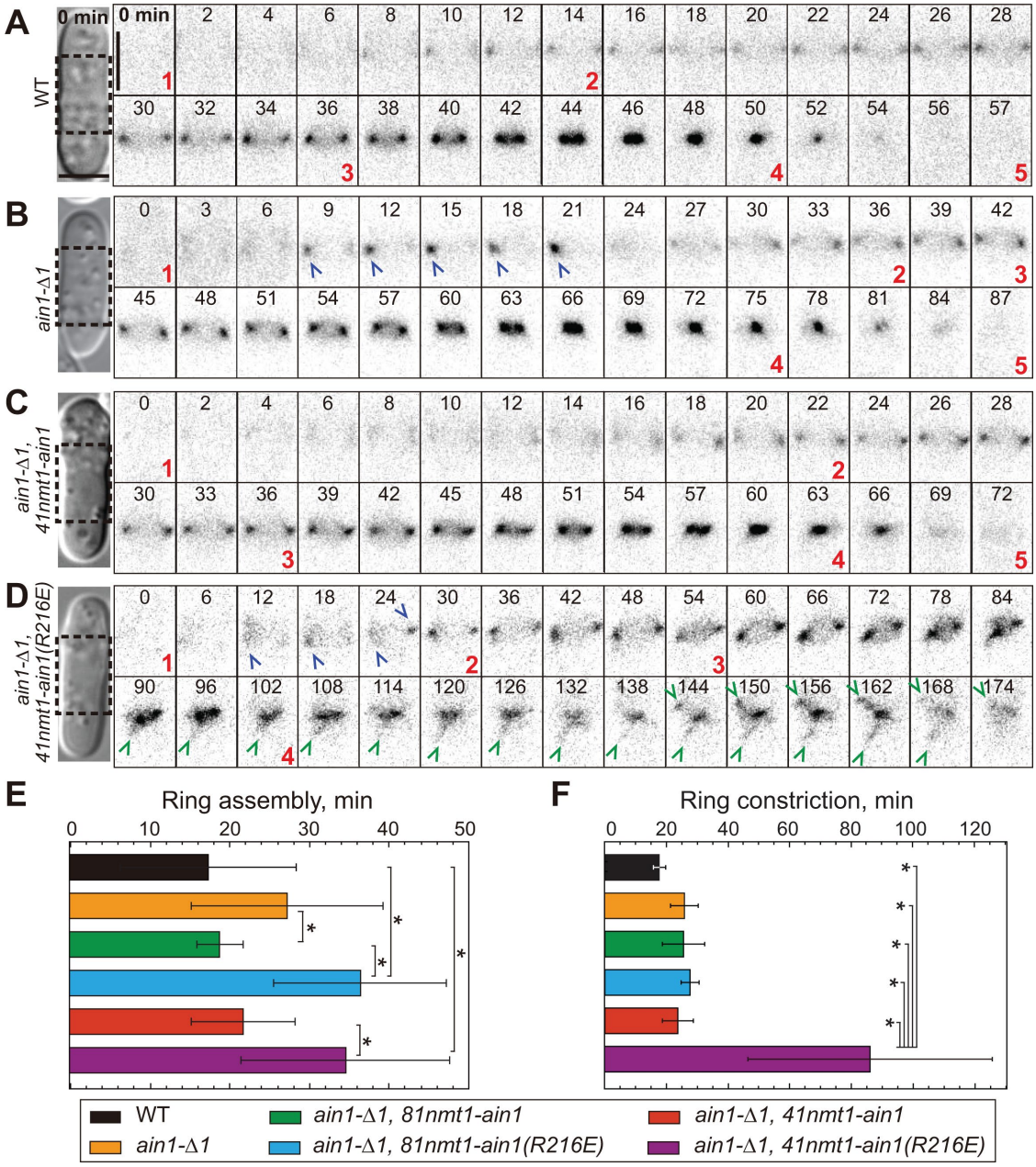

FIGURE 7: SpAin1(R216) causes defects in both contractile ring assembly and constriction. (A–F) Cytokinetic kinetics of WT cells, SpAin1 null *ain1-Δ1* cells, and *ain1-Δ1* cells expressing either WT SpAin1-GFP or mutant SpAin1(R216E)-GFP from low- (*81nmt1*) and medium- (*41nmt1*) strength promoters integrated at the *leu* locus. (A–D) Fluorescence micrograph montages of the time course of Rlc1-tdTomato–labeled contractile ring formation and constriction (right), corresponding to the boxed regions in DIC images (left). Cytokinetic stages are marked with red numbers as indicated in Supplemental Figure S7C: 1, Rlc1-tdTomato appearance (start); 2, ring assembly complete; 3, ring constriction begins; 4, ring constriction ends; 5, Rlc1-tdTomato disappears. Scale bars: 5 μm. (E) Average duration of ring assembly. Error bars, SD; $n \geq 10$ cells. *$p < 0.05$. (F) Average duration of ring constriction. Error bars, SD; $n \geq 10$ cells. *$p < 0.05$.

varying the affinity (K_d^{-1}) of SpAin1 for actin filaments, (see Supplemental Materials and Methods). In the simulation, each of two nodes elongates a single actin filament in the direction of the opposing node at either a 15°, 25°, or 35° angle relative to the axis connecting the two nodes, and the rate of first-filament capture by an opposing node is determined (Figure 8, C and D, and Supplemental Video 9). At 15°, filament capture occurs rapidly at low to middle cross-linker affinity (Figure 8D, black circles), as the filaments are already elongating in the approximate direction of the target nodes. However, as the filament angle increases away from the opposing node, lower rates of capture are observed at low cross-linker affinity, with capture increasing as the cross-linker affinity increases (Figure 8D, red squares and blue triangles). Optimum filament capture occurs at a middle affinity range, where K_d^{-1} is 0.1–0.3. This result demonstrates that cross-linkers increase the efficiency of filament capture, specifically when the actin filament is elongated at angles oriented farther from the target node. Conversely, at all angles tested, a high cross-linker affinity results in low- to no-node capture as filaments become

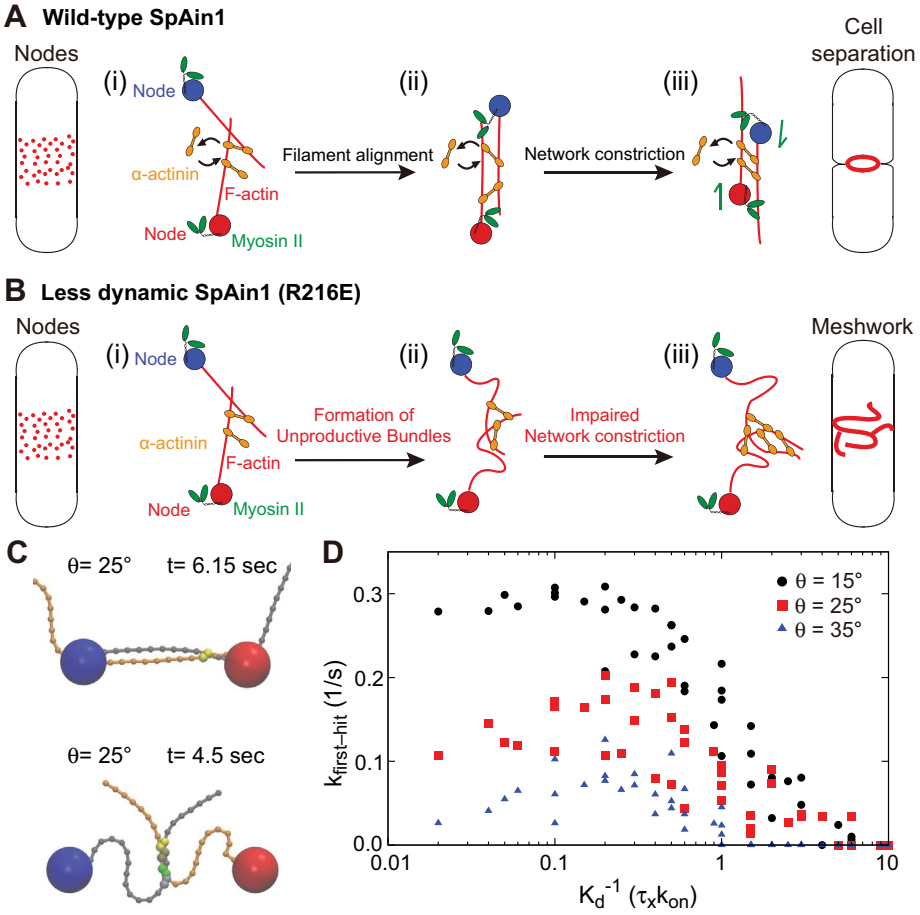

FIGURE 8: The role of dynamic SpAin1 during contractile ring assembly. (A and B) Cartoon model for SpAin1-mediated contractile ring assembly and constriction. (A) Condensation of pre ring nodes (red and blue circles) into a contractile ring by the SCPR model in a wild-type cell (Vavylonis *et al.*, 2008). Actin filaments assembled from nodes in random orientations are aligned into antiparallel bundles by SpAin1 (α-actinin) (i), which allows filaments to be efficiently captured by myosin-II motors on adjacent nodes (ii). The dynamic nature of SpAin1 allows myosin II to pull actin filaments without impediment, promoting proper ring constriction (iii). (B) Contractile ring formation in a cell expressing the less dynamic bundling mutant SpAin1(R216E). Actin filaments are elongated from nodes in random orientations (i), but get stalled as a result of excessive bundling, preventing actin filaments from reaching neighboring nodes (ii and iii). (C and D) Simulation of node capture at varying cross-linker affinities for F-actin (unitless K_d^{-1}). (C) Examples of node search and capture at low (0.3) cross-linker affinity (top) or high (3.0) cross-linker affinity (bottom). (D) Dependence of node capture rate ($k_{first\text{-}hit}$ (s^{-1})) over a range of cross-linker affinities (τ_x k_{on}) at filament elongation angles of 15° (black circles), 25° (red squares), or 35° (blue triangles) from the axis connecting the two nodes.

excessively cross-linked, leading to stalling of the cross-linked network and buckling of the elongating filaments (Figure 8C, bottom, and Supplemental Video 9, bottom). This result demonstrates that a dynamic cross-linker is necessary to prevent excessive interactions between filaments that may prevent filament capture by neighboring nodes. Though we suspect that a dynamic cross-linker's primary role is in enhancing filament capture by neighboring nodes, it is likely also important for allowing rapid ring constriction (Figure 8, Aiii and Biii), as our in vivo results and the work of others have shown that constriction is also slowed in the presence of less dynamic or excess cross-linkers (Mishra *et al.*, 2013). In particular, myosin II may be unable to contract actin filaments bundled by SpAin1(R216E) as a result of SpAin1(R216E)'s prolonged residence time. In support of this model, SpAin1(R216E) and *myo2-E1* double mutant cells have synthetic cell division defects compared with the single mutants alone (Supplementary Figure S8).

In this study, we have identified the importance of a dynamic cross-linker on proper contractile ring formation and constriction by examining the biochemical characteristics and in vivo function of *S. pombe* α-actinin SpAin1. In mammalian cells, human α-actinin HsACTN4 displays different fluorescence resonance energy transfer recovery times on stress fibers versus the cleavage furrow (Fraley *et al.*, 2005; Hotulainen and Lappalainen, 2006; Mukhina *et al.*, 2007), suggesting that its dynamics may be influenced by other actin-binding proteins or posttranslational modifications. Future work will involve determining how SpAin1 functions with other contractile ring actin-binding proteins such as tropomyosin to facilitate proper ring dynamics and how other actin-binding proteins may modify SpAin1's association with the contractile ring.

MATERIALS AND METHODS

DNA constructs for protein expression in insect cells

Insect cell expression constructs for full-length SpAin1 (pAcSG2-SpAin1-His) were prepared by PCR amplification from synthesized SpAin1 cDNA in a pUC57 plasmid (GenScript, Piscataway, NJ) with iProof DNA polymerase (Bio-Rad, Hercules, CA). A 6×His tag was included at the carboxyl-terminus and cloned by restriction digest with enzymes *Xho*I and *Bgl*II into the pAcSG2 vector (BD Biosciences, San Jose, CA). The QuikChange Site-Directed Mutagenesis Kit (Stratagene, La Jolla, CA) was used to generate the R216E point mutant in the SpAin1 insect cell expression vector (pAcSG2-SpAin1(R216E)-His). All inserts were confirmed by sequencing. Bacterial expression constructs for human fascin HsFSCN1 (pGEX-4T-3-fascin) and SpFim1 (pET21a-SpFim1p-His) have been described (Vignjevic *et al.*, 2006; Skau and Kovar, 2010).

Protein purification

Human fascin HsFSCN1 was purified by affinity chromatography from an extract of BL21-Codon Plus(DE3)-RP *E. coli* (Stratagene, La Jolla, CA) expressing pGEX-4T-3-fascin as described (Vignjevic *et al.*, 2006). SpFim1 was purified from bacteria by Talon metal affinity chromatography (Clontech, Mountain View, CA) and by a Source Q column (GE Healthcare Life Sciences, Pittsburgh, PA) as previously described (Skau and Kovar, 2010). HsACTN4 was expressed in *E. coli* BL21-Codon Plus(DE3)-RP by induction with 0.5 mM isopropyl β-D-thiogalactopyranoside (Sigma-Aldrich, St. Louis, MO) for 16 h at 16°C. Bacterial pellets were collected by centrifugation and resuspended in extraction buffer (50 mM NaH_2PO_4, pH 8.0, 500 mM NaCl, 10% glycerol, 10 mM imidazole, 10 mM β-mercaptoethanol [βME]) with 0.5 mM phenylmethylsulfonyl fluoride and 10 μg/l leupeptin and pepstatin (Sigma-Aldrich, St. Louis, MO). Resuspended pellets were homogenized

by being passed through an Emulsiflex-C3 (Avestin, Ottawa, ON, Canada). The lysate was clarified by centrifugation at 30,000 × *g* and 50,000 × *g*, and incubated with Talon metal affinity resin for 1 h at 4°C to bind 6xHis-tagged proteins. Protein was eluted with Talon elution buffer (50 mM NaH_2PO4, pH 8.0, 500 mM NaCl, 10% glycerol, 250 mM imidazole, 10 mM βME) and dialyzed overnight into Source Q buffer (20 mM Tris-HCl, pH 8.5, 50 mM NaCl, 5% glycerol, 0.01% NaN_3, 1 mM dithiothreitol [DTT]). Dialyzed protein was loaded onto a 5.0 ml Source Q column and eluted with a linear gradient from 300 to 700 mM NaCl in Source Q buffer. Pure HsACTN4 was dialyzed into α-actinin storage buffer (20 mM Tris-HCl, pH 7.9, 100 mM NaCl, 0.2 mM EDTA, 0.01% NaN_3, 1 mM DTT, and 10% glycerol), flash frozen, and stored at –80°C.

Full-length SpAin1 and SpAin1(R216E) were expressed in High Five insect cells via a baculovirus expression system, and isolated from High Five insect cells lysate by Talon affinity column as described above. For obtaining virus, Sf9 cells at 2×10^6/ml were co-transformed with the pAcSG2-based expression vector mixed with Sapphire linearized baculovirus DNA (Allele biotechnology, San Diego, CA) in Cellfectin transfection reagent (Life Technologies, Grand Island, NY). After transfected cells were incubated for 7 d, cells were pelleted by centrifugation, and the virus-containing supernatant was collected as primary transfection stock P1. A secondary stock, P2, was prepared by amplifying the primary stock. For protein purification, High Five insect cells at 2×10^6/ml were grown in serum-free Insect-Xpress media (Lonza, Allendale, NJ) transfected with P2 virus at a 1:1000 virus:cells ratio and incubated on a rotating platform for 72 h at 25°C. Cells were harvested by centrifugation at 4500 rpm for 10 min and resuspended in extraction buffer (25 mM HEPES, 10% glycerol, 10 mM imidazole, 400 mM KCl, 0.01% NaN_3, 10 mM βME, 0.5 mM PMSF and 10 μg/l leupeptin and pepstatin, pH 7.5). Resuspended cells were sheared in a dounce homogenizer (Kimble/Kontes Glass, Vineland, NJ) on ice 15 times and centrifuged at 15,000 rpm for 30 min. The supernatant lysate was diluted with an equal volume of extraction buffer without KCl (final 200 mM KCl). Protein was extracted from the lysate by Talon metal affinity resin as described above. Purified protein was dialyzed into α-actinin storage buffer, flash frozen, and stored at –80°C.

For gel-filtration chromatography, proteins were concentrated to ≥0.5 mg/ml and passed through a HiPrep 16/60 Sephacryl S-400 HR column (GE Healthcare, Pittsburgh, PA) equilibrated with 50 mM KCl, 1 mM $MgCl_2$, 1 mM ethylene glycol tetraacetic acid (EGTA), and 10 mM imidazole (pH 7.0), and 0.5 ml fractions were collected.

Protein concentrations were determined with extinction coefficients estimated from amino acid sequences with ProtParam (http://web.expasy.org/protparam): SpAin1/SpAin1(R216E) (A_{280} = 86,477 M^{-1} cm^{-1}), HsACTN4 (A_{280} = 125,500 M^{-1} cm^{-1}), SpFim1 (A_{280} = 55,140 M^{-1} cm^{-1}), and fascin (A_{280} = 68,152 M^{-1} cm^{-1}).

Ca-ATP actin was extracted from rabbit skeletal muscle acetone powder (Pel-Freez, Rogers, AR) by multiple rounds of assembly and disassembly as previously described (Spudich and Watt, 1971; Neidt *et al.*, 2008) and labeled on Cys-374 with Oregon Green 488 (Life Technologies, Carlsbad, CA) for TIRFM experiments as previously described (Kuhn and Pollard, 2005). Ca-ATP actin was converted to Mg-ATP actin immediately before each experiment by adding 0.1 volumes of 10 mM EGTA and 0.5 mM $MgCl_2$ for 2 min at 25°C.

Protein labeling

SpAin1, SpAin1(R216E), and HsACTN4 were labeled at cysteine sites using TMR-6-maleimide (Life Technologies, Carlsbad, CA) as previously described with a few modifications (Kovar *et al.*, 2001). Purified proteins were first dialyzed overnight into labeling buffer (20 mM Tris-HCl, pH 7.9, 100 mM NaCl, 0.2 mM EDTA, 0.01% NaN_3, and 10% glycerol) to remove DTT. TMR-6-maleimide was added to dialyzed proteins at 10-fold molar excess and incubated for 16 h at 4°C. After the coupling reaction was stopped with 1 mM DTT, samples were incubated with Talon metal affinity resin and loaded onto a disposable column. Resin was washed with Talon extraction buffer, and proteins were eluted with Talon elution buffer. Eluted fractions were measured at A_{280} and A_{555} for protein and TMR (A_{555} = 95,000 M^{-1} cm^{-1}) concentration. Labeled fractions were pooled, dialyzed, and stored in α-actinin buffer at 4°C.

Low- and high-speed actin filament sedimentation

Most nonmuscle α-actinins contain two EF-hand motifs downstream of the SRs that bind calcium and inhibit α-actinin's ability to bind F-actin (Noegel *et al.*, 1987; Tang *et al.*, 2001). SpAin1 contains two putative EF-hand motifs that are not expected to bind calcium (Wu *et al.*, 2001), so all of our in vitro experiments were performed with a low concentration of calcium (≤0.06 mM). Sedimentation assays were performed as previously described (Skau and Kovar, 2010). A sample of 15 μM Mg-ATP actin monomers were spontaneously assembled in 10 mM imidazole (pH 7.0), 50 mM KCl, 1 mM $MgCl_2$, 1 mM EGTA, 0.5 mM DTT, 0.2 mM ATP, and 90 μM $CaCl_2$ for 1 h to generate filaments. F-actin was then incubated with α-actinin for 20 min at 25°C and spun at 100,000 × *g* (high-speed) or 10,000 × *g* (low-speed) at 25°C. Supernatant and pellets were separated by 12.5% SDS–PAGE and stained with Coomassie blue for 30 min, destained for 16 h, and analyzed by densitometry on an Odyssey Infrared Imager (Li-Cor Biosciences, Lincoln, NE).

Microscopy of fluorescently labeled actin filaments

Bundles were obtained by incubating cross-linkers with preassembled F-actin, as described for sedimentation assays. At 20 min after incubation, 3 μl samples were carefully transferred to a new tube with cut pipette tips to minimize shearing. A sample of 15 μl of 1 μM TRITC-phalloidin (Sigma-Aldrich, St. Louis, MO) was added to the sample and incubated for 5 min to stop the reaction and fix filaments. Samples were diluted with 250 μl of fluorescence buffer (50 mM KCl, 1 mM $MgCl_2$, 100 mM DTT, 20 μg/ml catalase, 100 μg/ml glucose oxidase, 3 mg/ml glucose, 0.5% methyl cellulose [15 centipoises] and 10 mM imidazole, pH 7.0), and transferred to coverslips coated with 0.05 μg/μl poly-L-lysine. The concentration of cross-linkers used in each reaction was optimized to easily identify bundles by microscopy. Still images were collected with a charge-coupled device camera (Orca-ER, Hamamatsu, Bridgewater, NJ) on an Olympus IX-81 microscope.

TIRFM imaging of actin filaments

TIRFM images were collected with an Olympus IX-50 microscope fit with through-the-objective TIRF illumination and an iXon EMCCD camera (Andor Technology, South Windsor, CT) as previously described (Winkelman *et al.*, 2014). Conditions: 10 mM imidazole (pH 7.0), 50 mM KCl, 1 mM $MgCl_2$, 1 mM EGTA, 50 mM DTT, 0.2 mM ATP, 50 μM $CaCl_2$, 15 mM glucose, 20 μg ml^{-1} catalase, 100 μg ml^{-1} glucose oxidase, and 0.5% (400 cp) methycellulose. Coverslips and slides were washed in acetone for 30 min, in ethanol for 10 min, and then with Hellmanex III detergent (Hellma Analytics, Müllheim, Germany) for 2 h with sonication. Coverslips and slides were then incubated in piranha solution (66.6% H_2SO_4, 33.3% H_2O_2) for 2 h, in 1 M KOH for 30 min, and rinsed well in deionized H_2O. Air-dried glasses were coated with 1 mg/ml mPeg-Silane (5000 MW) in 95% ethanol (pH 2.0) for 16 h in the dark. To make flow chambers,

coverslips were double-taped down onto slides, creating chambers between parallel strips of tape (Winkelman *et al.*, 2014). Labeled F-actin was imaged in the 488-nm channel, and labeled α-actinins in the 561-nm channel. In spontaneous actin assembly TIRFM assays, unlabeled Mg-ATP actin and 33.3% Mg-ATP Oregon Green-actin were mixed with cross-linkers and transferred to a flow cell for imaging at 10 s intervals. For seeded TIRFM assays, seeds were prepared by preassembling F-actin from 15 μM Mg-ATP actin monomers (10% Oregon Green–labeled) for 1 h at 25°C and then incubated with cross-linkers for 20 min at 25°C. Tenfold-diluted samples were flowed into a reaction chamber coated with *N*-ethylmaleimide (NEM)-myosin II. After the flow cell was washed three times with 1× TIRF buffer, 0.75 μM Mg-ATP actin monomers (33.3% labeled with Oregon Green) were flowed into the cells to initiate elongation.

Quantification of residence time

Actin filaments were spontaneously assembled into bundles in the presence of optimal concentrations of cross-linkers to maximize the formation of two- and three-filament bundles. Bundling events were monitored from time = 0 to identify all filaments in the bundle by the number of elongating barbed ends. Pixel intensity was measured to confirm that two- and three-filament bundles have two to three times the fluorescence intensity of individual filaments. Fast-acquisition time-lapse movies were taken at 250 ms intervals with constant exposure. For determining the distribution of residence times, labeled α-actinin speckles were traced to measure the time between appearance and disappearance. Appearance was confirmed by a fluorescence level at least 1.5-fold above background. A single exponential equation, $f(t) = x_0 \times \exp^{(-t/T)}$, was used to fit 1-cumulative frequency to determine the residence time (T, mean lifetime of speckles on F-actin bundles; x_0, initial percent of bound speckles; t, time; $f(t)$, percent of bound speckles at time t). For fluorescence intensity measurements, the background fluorescence was subtracted with ImageJ using the rolling-ball method with a radius of 50 pixels (Winkelman *et al.*, 2014). The total fluorescence of each speckle was measured by ImageJ with a 3 pixel–radius circle centered at the speckle.

S. pombe strains, growth conditions, and cell microscopy

Table S1 lists the *S. pombe* strains used in this study. All tagged genes are either under the control of their endogenous promoters or integrated at the indicated loci under the control of *nmt1* promoters with different expression levels. SpAin1 and SpAin1(R216E) with either *41nmt1* or *81nmt1* promoters are integrated at the LEU+ locus. SpAin1 or SpAin1(R216E) were PCR-amplified from pAcSG2-SpAin1-His or pAcSG2-SpAin1(R216E)-His with restriction sites *Sac*II and *Not*I attached to the 5′ and 3′ ends. The PCR products and pJK148-Pnmt1-GFPc vector, which carries a thiamine-repressible *nmt1* promoter and a C-terminal GFP tag, were digested by restriction enzymes *Sac*II and *Not*I. Digested DNA was ligated by T4 ligase (New England BioLabs, Ipswich, MA) and linearized by digestion at an *Nru*I site within the *LEU+* gene. Digested ligation product was directly transformed into wild-type cells by lithium acetate transformation, and colonies were selected based on viability on medium lacking leucine and confirmed by diagnostic PCR. Strains integrated with SpAin1 or SpAin1(R216E) were then crossed to an *ain1-Δ1*, *rlc1-tdTomato* strain (KV628).

For live-cell microscopy, cells were grown in liquid YE5S (yeast extract plus five supplements complete) medium for 24 h at 25°C, washed four times in minimal EMM5S (Edinburgh minimal medium plus five supplements) to remove thiamine, and grown in EMMS at 25°C for 24 h to induce expression of *nmt1* promoters. For experiments involving temperature-sensitive myo2-E1 strains, cells were grown at 25°C in EMM5S and shifted to 28°C for 4 h before methanol fixation. DIC and epifluorescence images were obtained on an Orca-ER camera (Hamamatsu, Bridgewater, NJ) on an IX-81 microscope (Olympus, Tokyo, Japan) with a 60×, 1.4 numerical aperture Plan-Apo objective. For visualization of nuclei and septal material, cells were fixed in methanol and incubated with DAPI (nuclei) and calcofluor (septa) as described previously (Kovar *et al.*, 2003). Live-cell microscopy images of Rlc1-tdTomato and Ain1-GFP were collected in CellASic microfluidic chambers using The ONIX Microfluidic Perfusion Platform (EMD Millipore, Billerica, MA). Time-lapse images were acquired every minute with z-stacks spanning the cell depth with slices 0.5 μm apart.

GFP intensity was measured by the raw average pixel intensity in the measured region subtracting the average of 10 random boxes in the background. The boxes used for normalization were the same size as the measured region.

Computational model

Details of the computational model are described in the Supplemental Material.

ACKNOWLEDGMENTS

We thank Erin Adams (University of Chicago) and her lab for help with purification of SpAin1 from insect cells, William Brieher (University of Illinois, Urbana–Champaign) for kindly providing the bacterial expression plasmid of HsACTN4, and Jian-Qiu Wu (Ohio State University) and Matt Lord (University of Vermont) for fission yeast strains. G.M.H., G.A.V., and D.R.K. were supported in part by DOD/ARO through a MURI grant, number W911NF1410403, on which G.A.V. and D.R.K. are coinvestigators. This work is also supported by American Cancer Society RSG-11-126-01-CSM (to D.R.K.), National Institutes of Health (NIH) MCB Training Grant T32 GM0071832 (to J.R.C. and K.E.H.), NIH NRSA 1F32GM113415-01 (to G.M.H.) and NSF Graduate Student Fellowship DGE-1144082 (to J.R.C.). Computations were performed on resources at the Research Computing Center of the University of Chicago.

REFERENCES

Addario B, Sandblad L, Persson K, Backman L (2016). Characterisation of *Schizosaccharomyces pombe* a-actinin. Peer J e1858.

Andrianantoandro E, Pollard TD (2006). Mechanism of actin filament turnover by severing and nucleation at different concentrations of ADF/cofilin. Mol Cell 24, 13–23.

Bartles JR (2000). Parallel actin bundles and their multiple actin-bundling proteins. Curr Opin Cell Biol 12, 72–78.

Bathe M, Chang F (2009). Cytokinesis and the contractile ring in fission yeast: towards a systems-level understanding. Trends Microbiol 18, 38–45.

Bidone TC, Tang H, Vavylonis D (2014). Dynamic network morphology and tension buildup in a 3D model of cytokinetic ring assembly. Biophys J 107, 2618–2628.

Blanchard A, Ohanian V, Critchley D (1989). The structure and function of alpha-actinin. J Muscle Res Cell Motil 10, 280–289.

Borrego-Diaz E, Kerff F, Lee SH, Ferron F, Li Y, Dominguez R (2006). Crystal structure of the actin-binding domain of alpha-actinin 1: evaluating two competing actin-binding models. J Struct Biol 155, 230–238.

Breitsprecher D, Goode BL (2013). Formins at a glance. J Cell Sci 126, 1–7.

Broderick MJ, Winder SJ (2005). Spectrin, alpha-actinin, and dystrophin. Adv Protein Chem 70, 203–246.

Chen Q, Pollard TD (2011). Actin filament severing by cofilin is more important for assembly than constriction of the cytokinetic contractile ring. J Cell Biol 195, 485–498.

Coffman VC, Nile AH, Lee IJ, Liu H, Wu JQ (2009). Roles of formin nodes and myosin motor activity in Mid1p-dependent contractile-ring assembly during fission yeast cytokinesis. Mol Biol Cell 20, 5195–5210.

Courson DS, Rock RS (2010). Actin cross-link assembly and disassembly mechanics for alpha-actinin and fascin. J Biol Chem 285, 26350–26357.
Dandapani SV, Sugimoto H, Matthews BD, Kolb RJ, Sinha S, Gerszten RE, Zhou J, Ingber DE, Kalluri R, Pollak MR (2007). Alpha-actinin-4 is required for normal podocyte adhesion. J Biol Chem 282, 467–477.
Djinovic-Carugo K, Banuelos S, Saraste M (1997). Crystal structure of a calponin homology domain. Nat Struct Biol 4, 175–179.
Djinovic-Carugo K, Young P, Gautel M, Saraste M (1999). Structure of the alpha-actinin rod: molecular basis for cross-linking of actin filaments. Cell 98, 537–546.
Feng Y, Walsh CA (2004). The many faces of filamin: a versatile molecular scaffold for cell motility and signalling. Nat Cell Biol 6, 1034–1038.
Foley KS, Young PW (2013). An analysis of splicing, actin-binding properties, heterodimerization and molecular interactions of the non-muscle alpha-actinins. Biochem J 452, 477–488.
Fraley TS, Pereira CB, Tran TC, Singleton C, Greenwood JA (2005). Phosphoinositide binding regulates alpha-actinin dynamics: mechanism for modulating cytoskeletal remodeling. J Biol Chem 280, 15479–15482.
Fujiwara K, Porter ME, Pollard TD (1978). Alpha-actinin localization in the cleavage furrow during cytokinesis. J Cell Biol 79, 268–275.
Galkin VE, Orlova A, Salmazo A, Djinovic-Carugo K, Egelman EH (2010). Opening of tandem calponin homology domains regulates their affinity for F-actin. Nat Struct Mol Biol 17, 614–616.
Goyal A, Takaine M, Simanis V, Nakano K (2011). Dividing the spoils of growth and the cell cycle: the fission yeast as a model for the study of cytokinesis. Cytoskeleton (Hoboken) 68, 69–88.
Hampton CM, Taylor DW, Taylor KA (2007). Novel structures for alpha-actinin:F-actin interactions and their implications for actin-membrane attachment and tension sensing in the cytoskeleton. J Mol Biol 368, 92–104.
Honda K, Yamada T, Hayashida Y, Idogawa M, Sato S, Hasegawa F, Ino Y, Ono M, Hirohashi S (2005). Actinin-4 increases cell motility and promotes lymph node metastasis of colorectal cancer. Gastroenterology 128, 51–62.
Hotulainen P, Lappalainen P (2006). Stress fibers are generated by two distinct actin assembly mechanisms in motile cells. J Cell Biol 173, 383–394.
Ishikawa R, Sakamoto T, Ando T, Higashi-Fujime S, Kohama K (2003). Polarized actin bundles formed by human fascin-1: their sliding and disassembly on myosin II and myosin V in vitro. J Neurochem 87, 676–685.
Kamasaki T, Osumi M, Mabuchi I (2007). Three-dimensional arrangement of F-actin in the contractile ring of fission yeast. J Cell Biol 178, 765–771.
Kaplan JM, Kim SH, North KN, Rennke H, Correia LA, Tong HQ, Mathis BJ, Rodriguez-Perez JC, Allen PG, Beggs AH, Pollak MR (2000). Mutations in ACTN4, encoding alpha-actinin-4, cause familial focal segmental glomerulosclerosis. Nat Genet 24, 251–256.
Kovar DR, Gibbon BC, McCurdy DW, Staiger CJ (2001). Fluorescently-labeled fimbrin decorates a dynamic actin filament network in live plant cells. Planta 213, 390–395.
Kovar DR, Kuhn JR, Tichy AL, Pollard TD (2003). The fission yeast cytokinesis formin Cdc12p is a barbed end actin filament capping protein gated by profilin. J Cell Biol 161, 875–887.
Krause M, Dent EW, Bear JE, Loureiro JJ, Gertler FB (2003). Ena/VASP proteins: regulators of the actin cytoskeleton and cell migration. Annu Rev Cell Dev Biol 19, 541–564.
Kuhn JR, Pollard TD (2005). Real-time measurements of actin filament polymerization by total internal reflection fluorescence microscopy. Biophys J 88, 1387–1402.
Laporte D, Ojkic N, Vavylonis D, Wu JQ (2012). Alpha-actinin and fimbrin cooperate with myosin II to organize actomyosin bundles during contractile-ring assembly. Mol Biol Cell 23, 3094–3110.
Lee IJ, Coffman VC, Wu JQ (2012). Contractile-ring assembly in fission yeast cytokinesis: recent advances and new perspectives. Cytoskeleton (Hoboken) 69, 751–763.
Liu J, Taylor DW, Taylor KA (2004). A 3-D reconstruction of smooth muscle alpha-actinin by CryoEm reveals two different conformations at the actin-binding region. J Mol Biol 338, 115–125.
Lord M, Pollard TD (2004). UCS protein Rng3p activates actin filament gliding by fission yeast myosin-II. J Cell Biol 167, 315–325.
Low SH, Mukhina S, Srinivas V, Ng CZ, Murata-Hori M (2010). Domain analysis of alpha-actinin reveals new aspects of its association with F-actin during cytokinesis. Exp Cell Res 316, 1925–1934.
Lu J, Pollard TD (2001). Profilin binding to poly-L-proline and actin monomers along with ability to catalyze actin nucleotide exchange is required for viability of fission yeast. Mol Biol Cell 12, 1161–1175.
Mabuchi I, Hamaguchi Y, Kobayashi T, Hosoya H, Tsukita S, Tsukita S (1985). Alpha-actinin from sea urchin eggs: biochemical properties, interaction with actin, and distribution in the cell during fertilization and cleavage. J Cell Biol 100, 375–383.
Matsudaira P (1991). Modular organization of actin crosslinking proteins. Trends Biochem Sci 16, 87–92.
Meyer RK, Aebi U (1990). Bundling of actin filaments by alpha-actinin depends on its molecular length. J Cell Biol 110, 2013–2024.
Mishra M, Kashiwazaki J, Takagi T, Srinivasan R, Huang Y, Balasubramanian MK, Mabuchi I (2013). In vitro contraction of cytokinetic ring depends on myosin II but not on actin dynamics. Nat Cell Biol 15, 853–859.
Mukhina S, Wang YL, Murata-Hori M (2007). Alpha-actinin is required for tightly regulated remodeling of the actin cortical network during cytokinesis. Dev Cell 13, 554–565.
Nakano K, Satoh K, Morimatsu A, Ohnuma M, Mabuchi I (2001). Interactions among a fimbrin, a capping protein, and an actin-depolymerizing factor in organization of the fission yeast actin cytoskeleton. Mol Biol Cell 12, 3515–3526.
Neidt EM, Skau CT, Kovar DR (2008). The cytokinesis formins from the nematode worm and fission yeast differentially mediate actin filament assembly. J Biol Chem 283, 23872–23883.
Noegel A, Witke W, Schleicher M (1987). Calcium-sensitive non-muscle alpha-actinin contains EF-hand structures and highly conserved regions. FEBS Lett 221, 391–396.
Ojkic N, Vavylonis D (2010). Kinetics of myosin node aggregation into a contractile ring. Phys Rev Lett 105, 048102.
Ojkic N, Wu JQ, Vavylonis D (2011). Model of myosin node aggregation into a contractile ring: the effect of local alignment. J Phys Condens Matter 23, 374103.
Otto JJ (1994). Actin-bundling proteins. Curr Opin Cell Biol 6, 105–109.
Rajfur Z, Roy P, Otey C, Romer L, Jacobson K (2002). Dissecting the link between stress fibres and focal adhesions by CALI with EGFP fusion proteins. Nat Cell Biol 4, 286–293.
Roca-Cusachs P, del Rio A, Puklin-Faucher E, Gauthier NC, Biais N, Sheetz MP (2013). Integrin-dependent force transmission to the extracellular matrix by alpha-actinin triggers adhesion maturation. Proc Natl Acad Sci USA 110, E1361–E1370.
Saha S, Pollard TD (2012). Characterization of structural and functional domains of the anillin-related protein Mid1p that contribute to cytokinesis in fission yeast. Mol Biol Cell 23, 3993–4007.
Sanger JM, Mittal B, Pochapin MB, Sanger JW (1987). Stress fiber and cleavage furrow formation in living cells microinjected with fluorescently labeled alpha-actinin. Cell Motil Cytoskeleton 7, 209–220.
Shao H, Wang JH, Pollak MR, Wells A (2010). Alpha-actinin-4 is essential for maintaining the spreading, motility and contractility of fibroblasts. PLoS One 5, e13921.
Sjoblom B, Salmazo A, Djinovic-Carugo K (2008). Alpha-actinin structure and regulation. Cell Mol Life Sci 65, 2688–2701.
Skau CT, Courson DS, Bestul AJ, Winkelman JD, Rock RS, Sirotkin V, Kovar DR (2011). Actin filament bundling by fimbrin is important for endocytosis, cytokinesis and polarization in fission yeast. J Biol Chem 286, 26964–26977.
Skau CT, Kovar DR (2010). Fimbrin and tropomyosin competition regulates endocytosis and cytokinesis kinetics in fission yeast. Curr Biol 20, 1415–1422.
Skau CT, Neidt EM, Kovar DR (2009). Role of tropomyosin in formin-mediated contractile ring assembly in fission yeast. Mol Biol Cell 20, 2160–2173.
Spudich JA, Watt S (1971). The regulation of rabbit skeletal muscle contraction. I. Biochemical studies of the interaction of the tropomyosin-troponin complex with actin and the proteolytic fragments of myosin. J Biol Chem 246, 4866–4871.
Stachowiak MR, Laplante C, Chin HF, Guirao B, Karatekin E, Pollard TD, O'Shaughnessy B (2014). Mechanism of cytokinetic contractile ring constriction in fission yeast. Dev Cell 29, 547–561.
Sun L, Guan R, Lee IJ, Liu Y, Chen M, Wang J, Wu JQ, Chen Z (2015). Mechanistic insights into the anchorage of the contractile ring by anillin and Mid1. Dev Cell 33, 413–426.
Tang VW, Brieher WM (2012). Alpha-actinin-4/FSGS1 is required for Arp2/3-dependent actin assembly at the adherens junction. J Cell Biol 196, 115–130.
Tang J, Taylor DW, Taylor KA (2001). The three-dimensional structure of alpha-actinin obtained by cryoelectron microscopy suggests a model for Ca^{2+}-dependent actin binding. J Mol Biol 310, 845–858.

Taylor KA, Taylor DW, Schachat F (2000). Isoforms of alpha-actinin from cardiac, smooth, and skeletal muscle form polar arrays of actin filaments. J Cell Biol 149, 635–646.
Vavylonis D, Wu JQ, Hao S, O'Shaughnessy B, Pollard TD (2008). Assembly mechanism of the contractile ring for cytokinesis by fission yeast. Science 319, 97–100.
Vignjevic D, Peloquin J, Borisy GG (2006). In vitro assembly of filopodia-like bundles. Methods Enzymol 406, 727–739.
Virel A, Backman L (2004). Molecular evolution and structure of alpha-actinin. Mol Biol Evol 21, 1024–1031.
Virel A, Backman L (2006). Characterization of *Entamoeba histolytica* alpha-actinin. Mol Biochem Parasitol 145, 11–17.
Virel A, Backman L (2007). A comparative and phylogenetic analysis of the alpha-actinin rod domain. Mol Biol Evol 24, 2254–2265.
Wachsstock DH, Schwartz WH, Pollard TD (1993). Affinity of alpha-actinin for actin determines the structure and mechanical properties of actin filament gels. Biophys J 65, 205–214.
Ward SM, Weins A, Pollak MR, Weitz DA (2008). Dynamic viscoelasticity of actin cross-linked with wild-type and disease-causing mutant alpha-actinin-4. Biophys J 95, 4915–4923.
Weins A, Kenlan P, Herbert S, Le TC, Villegas I, Kaplan BS, Appel GB, Pollak MR (2005). Mutational and biological analysis of alpha-actinin-4 in focal segmental glomerulosclerosis. J Am Soc Nephrol 16, 3694–3701.
Weins A, Schlondorff JS, Nakamura F, Denker BM, Hartwig JH, Stossel TP, Pollak MR (2007). Disease-associated mutant alpha-actinin-4 reveals a mechanism for regulating its F-actin-binding affinity. Proc Natl Acad Sci USA 104, 16080–16085.
Winkelman JD, Bilancia CG, Peifer M, Kovar DR (2014). Ena/VASP Enabled is a highly processive actin polymerase tailored to self-assemble parallel-bundled F-actin networks with Fascin. Proc Natl Acad Sci USA 111, 4121–4126.
Wu JQ, Bahler J, Pringle JR (2001). Roles of a fimbrin and an alpha-actinin-like protein in fission yeast cell polarization and cytokinesis. Mol Biol Cell 12, 1061–1077.
Wu JQ, Kuhn JR, Kovar DR, Pollard TD (2003). Spatial and temporal pathway for assembly and constriction of the contractile ring in fission yeast cytokinesis. Dev Cell 5, 723–734.
Wu JQ, Sirotkin V, Kovar DR, Lord M, Beltzner CC, Kuhn JR, Pollard TD (2006). Assembly of the cytokinetic contractile ring from a broad band of nodes in fission yeast. J Cell Biol 174, 391–402.
Xu J, Wirtz D, Pollard TD (1998). Dynamic cross-linking by alpha-actinin determines the mechanical properties of actin filament networks. J Biol Chem 273, 9570–9576.
Ylanne J, Scheffzek K, Young P, Saraste M (2001). Crystal structure of the alpha-actinin rod: four spectrin repeats forming a tight dimer. Cell Mol Biol Lett 6, 234.